International Journal of Adhesion & Adhesives 139 (2025) 103979

Contents lists available at ScienceDirect

International Journal of Adhesion and Adhesives

journal homepage: www.elsevier.com/locate/ijadhadh

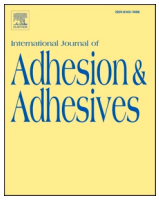

Slow-growth damage of bonded composite-metal joints subjected to fatigue loading

Laurence Wong [a], John Wang [b], Richard Chunhui Yang [a], Y.X. Zhang [a,*]

[a] Centre for Advanced Manufacturing Technology, School of Engineering, Design and Built Environment, Western Sydney University (WSU), NSW, 2751, Australia
[b] Platforms Division, Defence Science and Technology Group (DSTG), Melbourne, VIC, 3207, Australia

ARTICLE INFO

Keywords:
Adhesive bond
Composite joint
Fatigue testing
Finite element analysis
Slow-growth damage

ABSTRACT

This study investigates the slow-growth damage of bonded composite-metal (CFRP-Aluminium) hybrid double lap joints. First, static tension tests were conducted to measure the residual strength of the partially disbonded joints. Finite element models were developed to predict the residual strength as a function of disbond crack length. The model was calibrated using the static test results and the characteristic distance method. Then, constant amplitude fatigue tests were conducted at a practical load range, determined on the basis of joint static strength and safety factor requirements, to measure disbond growth rates and joint fatigue life. Further numerical analyses were conducted, where the extended finite element method (XFEM) and virtual crack closure technique (VCCT) were applied to predict energy release rates at the disbond crack tip of the joints. The crack growth rates measured from the fatigue tests and the energy release rates from the parametric numerical analyses consistently indicated that slow-growth behaviour was present. By combining the crack growth rates and energy release rates, modified Paris laws were established to predict the disbonded crack growth and fatigue life of the joints with satisfactory results obtained. In addition, an important observation was made, that is, in the fatigue tests the disbond from the taper end would not migrate to generate delamination, the mechanism of which was convincingly revealed by a detailed FEM analysis. This study successfully implemented the proposed framework for the slow growth damage prediction of adhesively bonded joints and demonstrated its effectiveness.

1. Introduction

Adhesive bonding exhibits excellent damage tolerance and fatigue resistance, as well as low weight and stress concentrations when compared to traditional mechanical fasteners [1,2]. Composites, such as carbon fibre reinforced polymers (CFRP), are widely used in aircraft structures due to their high strength and stiffness-to-weight ratio and fatigue resistance [3]. In aircraft design, the adhesive bonding of composites is often seen in the patch repairs of damaged parent structures, which typically feature a tapered edge to minimise adhesive shear and peel stresses and improve joint strength [4]. Adhesively bonded composite joints with fibre reinforced laminates have two primary critical failure modes, namely adhesive disbond and composite failure, such as delamination [5]. In the case of disbond, the damage propagates along the adhesive layer, reducing the contact between adherends.

Under the context of adhesively bonded composite joints, the Federal Aviation Administration (FAA) requires that primary aircraft structures are assessed with the appropriate damage tolerance criteria [6,7]. As summarised in the Composites Materials Handbook 17 [8], the non-damage-growth criterion works well for many fatigue non-sensitive composite structures. In these structures, damage growth under fatigue loading is often a sign revealing significant through-thickness stresses unanticipated during the design stage, and thus a redesign should be conducted. Likewise, repairs or replacements of damaged in-service structures are often required to restore static strength safety margins, well before the need to address fatigue performance concerns.

However, it has also long been recognised that in some damage cases, most typically delamination in laminates and disbond in bonded joints where the damage can grow under fatigue loading with a peak load well below 50 % of their static (residual) strength in shear or peel, a slow-growth management approach could apply [9]. Such a damage tolerance management strategy may be beneficial towards reducing maintenance costs by delaying or avoiding unnecessary repairs or replacement of composite components. Since 2010, this slow-growth management strategy has been considered acceptable by the FAA, provided the damage growth is predictable [6,8].

* Corresponding author.
E-mail address: sarah.zhang@westernsydney.edu.au (Y.X. Zhang).

https://doi.org/10.1016/j.ijadhadh.2025.103979
Received 31 July 2024; Received in revised form 4 February 2025; Accepted 7 February 2025
Available online 8 February 2025

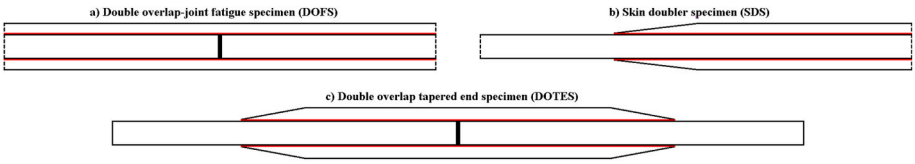

Fig. 1. Joint design of a) DOFS, b) SDS, and c) DOTES.

According to Chalkley et al. [10], the fatigue crack growth within the disbond-tolerant zone is slow and stable, whereas the safe-life zone (taper) exhibits rapid crack growth. As such, the composite-metal double overlap-joint fatigue specimen (DOFS), as shown in Fig. 1a, and skin doubler specimen (SDS), as shown in Fig. 1b, were proposed to examine the disbond-tolerant zone and the safe-life zone of a tapered bonded patch repair, respectively.

Much research has been reported on the fatigue crack propagation of adhesively bonded composite joints [11–16], composite double cantilever beams [17–22], and adhesively bonded metal joints [23–25]. While these studies examined the crack growth rates of adhesively bonded composite joints, a large majority of the research focused on crack initiation and propagation within a relatively short overlap length. Limited research was reported on the slow-growth damage behaviour of adhesively bonded joints under fatigue loading, which requires a sufficiently long overlap length. Some research on the slow-growth damage behaviour of adhesively bonded joints with relatively limited length or metal-metal joints were reported in the literatures. Wu et al. [26] evaluated composite-composite skin doubler repaired specimens with initial disbond cracks, and slow-growth damage was observed within the specimens until a crack length of 30 mm before accelerating until failure. Tanulia et al. [27] proposed the metal-metal double overlap tapered end specimen (DOTES), as shown in Fig. 1c, as a joint geometry, and assessed the slow-growth damage behaviour of a disbond crack within the adhesive layer owing to its long overlap length. Tanulia et al. [28] studied the growth behaviour of cracks from initiation to joint failure, and slow-growth damage was observed until a crack length of 150 mm for a joint with 180 mm overlap length. Further research must still be conducted for the certification of repair patches with cracks exhibiting slow-growth damage behaviours. However very scarce research has been conducted to investigate the slow-growth damage behaviours of bonded composite-metal hybrid joints and composite-composite joints although these two types of joints represent the most often used joints for bonded composite patch repairs or joint structures. With composite adherends under fatigue loading, delamination damage and delamination-disbond interaction could possibly be involved, which complicates the matter. Additionally, compressive loading is a critical load case for fibre reinforced composites [29], therefore anti-buckling must be adequately considered in fatigue compression tests, which is a significant challenge for the tests.

A comprehensive research framework is developed to examine the slow-growth damage behaviours of composite-metal hybrid joint in this paper. Preliminary research was conducted through finite element modelling of composite-metal hybrid joints and composite-composite joints with varying disbond and delamination crack lengths [30,31]. In this paper, the investigation of the bonded composite-metal hybrid double lap joints with disbond cracks originating from the taper end under fatigue loading is conducted by effective application of both experimental and numerical methods. With the completion of all five steps of this framework as listed below, this study can be used to inform the design and maintenance regimes of bonded composite aircraft structures.

1) Predicting the residual strength of the bonded joint as a function of disbond crack length through finite element analysis. The model is to be calibrated through the characteristic distance method using experimental residual strengths from static tests.
2) Acquiring the fatigue life and crack growth rates by conducting fatigue tests on bonded joints with varying pre-crack lengths. The upper limit of the fatigue peak load is calculated based on the predicted residual strength with knock-down factors and aluminium strength requirements. For the research to focus on practical use, the fatigue peak load should not exceed this value.
3) Predicting the energy release rate of the bonded joint as a function of disbond crack length through finite element analysis. The energy release rate for crack lengths corresponding to the experimentally measured cracks must also be attained.

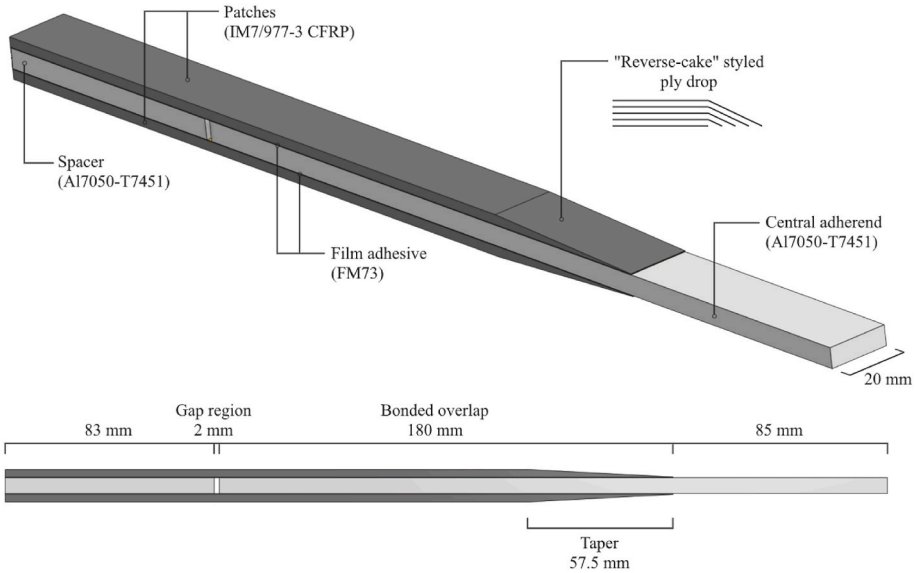

Fig. 2. Geometry of the composite-metal hybrid double lap joint.

Table 1
Material properties for Al 7050-T7451 [28].

E (GPa)	ν	σ_y (MPa)	σ_{UT} (MPa)
71.7	0.33	469	524

4) Establishing a modified Paris law – the relationship between experimentally measured crack growth rate and numerically predicted energy release rate.
5) Predicting the fatigue life of the bonded joint by determining the number of cycles needed for a crack of a particular length to grow until the residual strength of the bonded joint decreases to the fatigue peak load, resulting in subsequent failure. Accurate prediction of the crack growth at different crack length ranges against cycle number enables the overall prediction of the disbond crack growth behaviour throughout the entire overlap length.

This paper is structured with five main sections. Section 2 presents the details of the experimental programs, including joint design and static and fatigue testing. Section 3 describes the finite element modelling-based numerical programs. Section 4 presents the results and discussion for the experimental and numerical work. Section 5 combines experimental and numerical data to analytically predict the fatigue life of the adhesively bonded joints. Section 6 contains the conclusions and recommendations.

2. Methodology - experimental programs

To better understand the slow-growth behaviour of disbond cracks, bonded composite-metal hybrid double lap joints were designed, fabricated, and tested, as elaborated on in the following sub-sections.

2.1. Specimen design and preparation

The bonded composite-metal hybrid double lap joint investigated in this study is comprised of four different parts (central adherend, spacer, and two tapered patches) bonded together with layers of film adhesive. Fig. 2 illustrates the labelled geometry of the double lap joint designed in this study. In a practical application, bending within the aluminium plate is restricted by the surrounding material of the parent structure. As such, a balanced double lap joint configuration was considered instead, since a single lap joint would introduce a bending moment upon tensile loading. The spacer side and the exposed central adherend of the specimen were reserved for the testing machine to grip the specimens. A 2-mm gap was placed between the central adherend and the spacer to simulate a damaged parent structure while the bonded composite patches represented a joint structure or patch repair. The composite outer adherends consisted of 24 plies each with a thickness of 0.127 mm, while the central adherend had a thickness of 6.35 mm. The adhesive layers each consisted of two adhesive films, producing an overall thickness of 0.3 mm. To simulate pre-existing disbond cracks of different lengths, Teflon films of various lengths were embedded between the adhesive films starting from the tip of the taper.

Aluminium 7050-T7451 was selected for the central adherend and spacer. The outer adherends consisted of the IM7/977-3 carbon fibre reinforced polymer (CFRP) with a layup configuration of $[(-45/0_2/45/90)_2/\text{-}45/0]_s$. The adhesive used was FM 73 film adhesive. Tables 1–3 list the material properties of the Al 7050-T7451, IM7/977-3, and FM 73, respectively.

The surface treatment of the Al 7050-T7451 plates involved grit blasting and a 1 % aqueous epoxy-silane solution treatment, as detailed by Rider and Chalkley [36]. The surface treatment of the IM7/977-3 laminates consisted of abrasion using 300 grit (or finer) sandpaper and checking for wettability until fully wet. The surface was then cleaned using Methyl-Ethyl-Ketone, rinsed with demineralised water, and dried in an oven at 90 °C.

Static tensile tests were conducted on bonded joints with three taper disbond crack lengths of 60, 120, and 165 mm (two of each) to measure the residual strengths of the partially disbonded joints. Fatigue tension-tension tests were conducted on joints with taper disbond crack lengths of 60 (three) and 120 mm (two) to measure the disbond crack growth rates and fatigue life.

2.2. Static testing program

The bonded composite-metal hybrid double lap joints were tested under tensile loading until failure to acquire the static residual strengths of the joints. The static tests were performed in an Instron 5985 universal testing machine with Bluehill Universal software. The static test specimens were loaded at a crosshead displacement rate of 1 mm/min. Displacement and load measurements were recorded.

2.3. Fatigue testing program

The adhesively bonded composite-metal hybrid double lap joints were tested under fatigue loading using a CMA fatigue testing rig of 400-kN load capacity. The fatigue testing involved a constant amplitude sinusoidal loading regime with a frequency of 3 Hz and an R-ratio ($\sigma_{min}/\sigma_{max}$) of 0.1. To focus on practical application, three metrics for an upper fatigue peak load were considered. The three metrics are listed below.

- Numerical analysis was conducted to calculate the residual strength for a joint with a 10-mm disbond crack (assuming a typical NDI detectable initial disbond length). The numerical residual strength prediction of 79.9 kN with a cumulative knock-down factor of 0.48 (B-Basis (× 0.8), factor of safety (÷1.5), and hot-wet conditions (× 0.9) [28,30]) produces an upper fatigue limit of 38.4 kN.
- Applying a factor of safety of 1.5 to the Al 7050-T7451 yield strength of 469.0 MPa (Table 1) provides an upper fatigue limit of 312.7 MPa or 39.7 kN.
- The endurance limit of Al 7050-T7451 for a 5.0×10^5 cycle fatigue life is 275.0 MPa [37] or 35.0 kN.

The load of 35.0 kN, the lowest of the three limits, was considered as the applicable upper fatigue limit. Preliminary fatigue tests were conducted on joints with smaller disbond cracks (20 mm) with the joints experiencing aluminium failure with no visible disbond crack growth, suggesting that the taper played a significant role in reducing adhesive stresses. Since the scope of this study is on slow-growth behaviour, which requires longer crack lengths, specimens with disbond lengths of 60 and 120 mm from the taper end were tested with a fatigue load range

Table 3
Material properties for FM 73 [34,35].

E (MPa)	ν	τ_y (MPa)	τ_{max} (MPa)	γ_{max}	G_{Ic} (kJ/m^2)	G_{IIc} (kJ/m^2)
2160	0.35	32.3	40.9	0.853	2.5	5

Table 2
Material properties for IM7/977-3 [32,33].

E_1 (GPa)	E_2 (GPa)	E_3 (GPa)	ν_{12}	ν_{13}	ν_{23}	G_{12} (GPa)	G_{13} (GPa)	G_{23} (GPa)	G_{Ic} (kJ/m^2)	G_{IIc} (kJ/m^2)
164	9.86	9.86	0.33	0.33	0.34	4.95	4.95	2.94	0.256	0.649

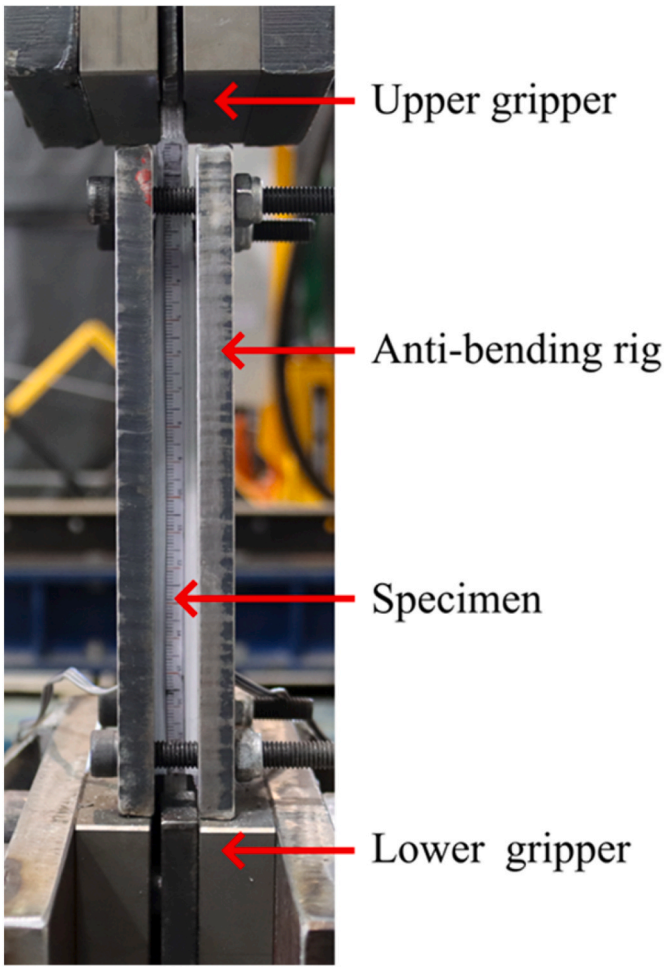

Fig. 3. Fatigue testing setup.

of 3.33–33.3 kN.

The front-facing sides of the fatigue specimens were painted white for contrast against the cracks and a scale was marked on the central adherend to measure the crack lengths within the adhesive layers. A Canon EOS 90D DSLR camera with 18–55 mm lens was used to photograph the specimen every 1000 cycles during its peak load to maximise the visibility of the crack opening. Additionally, an anti-bending fixture presented by Tanulia et al. [28] was used to decrease the presence of bending due to asymmetrical crack growth. Nyloc nuts were used to tighten the anti-bending fixture to prevent vibration loosening. However, the fixture still had the ability to slide vertically along the specimen, ensuring that there were no excessive forces acting on the specimen itself. Fig. 3 illustrates the fatigue testing setup.

3. Methodology – numerical modelling

In order to predict the residual strengths and energy release rates as a function of disbond crack length, 3D finite element models of the composite-metal hybrid double lap joints with taper end disbond cracks under tensile loading were created using Abaqus/CAE 2021. Additionally, numerical models of the joints with taper end disbond migrated to first-ply delamination cracks were created to quantify the non-migratory behaviour of a disbond crack in the presence of a delamination crack.

3.1. Finite element models

To consider the asymmetrical disbond crack growth within the double lap joints, a full model of the joint containing both outer

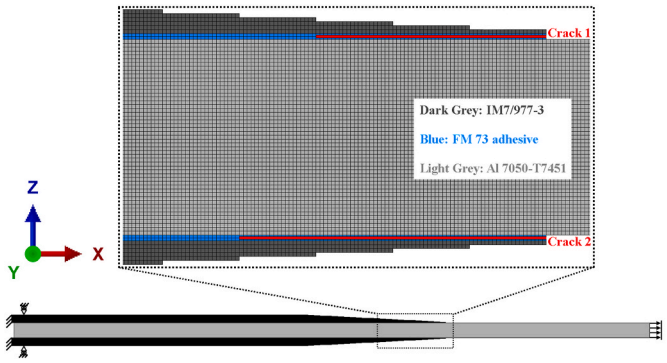

Fig. 4. Geometry of the finite element model.

adherends was created with the geometry shown in Fig. 4. The aluminium spacer in the experimental specimen (Fig. 2) was not included in the finite element model because it served only to provide length for the testing machine to grip the specimen. Although the CFRP plies in the physical joint were tapered in a 'reverse-cake' style (Fig. 2), the numerical model used a traditional cake styled ply-drop for simplicity.

The entirety of the model was discretised with three-dimensional 8-node hexahedral solid continuum elements (C3D8R). Each of the CFRP plies was modelled by one element, and the adhesive layers were discretised with two elements, through thickness. The 20-mm thick double lap joint was represented as a 1-mm thick numerical model with plane strain conditions. The plane strain conditions were applied by restricting the translation degree of freedom along the Y-axis (Fig. 4). With a global mesh size of 0.125 mm, the models had approximately 180,000 elements.

To evaluate the residual strengths of the double lap joints with various disbond crack lengths, it is necessary to determine the applied tensile load at the aluminium end during the instance when the shear strain within an adhesive element at the crack tip reached the maximum shear strain (Table 3). As such, the FM 73 film adhesive was modelled with an elastic-plastic material based on the true stress-true strain behaviours provided by Aydin [34]. In the calculation to determine the residual strength of the adhesive bonding of the joint, the IM7/977-3 and Al 7050-T7451 were modelled as linear elastic materials. Due to the orthotropic nature of the unidirectional IM7/977-3, the elements with orthotropic CFRP properties were given material orientations corresponding to their respective ply orientations. The Al 7050-T7451 and FM 73 were both modelled as isotropic materials. The mechanical properties of the materials are presented in Tables 1–3

3.2. Residual strength and energy release rate predictions

The prediction of adhesive stresses within the crack tip are sensitive to mesh size, particularly for elements immediately adjacent to the crack tip. A finer mesh resulted in a lower predicted residual strength. As such, traditional h- and p-refinement mesh convergences could not be used. Whitney and Nuismer [38] proposed a characteristic distance method to calculate the residual strength of a structure with a straight crack. As summarised in Refs. [28,39], this characteristic distance can be acquired by adjusting the crack tip element size until the numerically predicted and experimentally measured static residual strengths match. Through this method, an element size of 0.125 mm was determined that yielded a residual strength prediction matching the static test results. As the 0.3 mm thick adhesive layer was discretised by two elements (0.15 mm element size through thickness), this 0.125 mm was for the longitudinal element size.

Separate models were used to assess the energy release rates of the joints at different disbond crack lengths. To calculate the energy release rates, the finite element models utilised the virtual crack closure

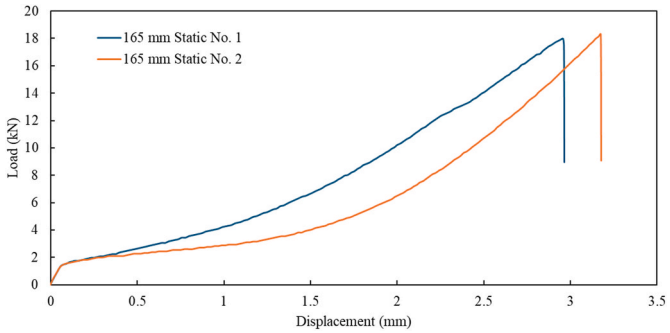

Fig. 5. Static residual strength of joints with 165-mm taper disbond cracks.

Table 4
Overview of the tested fatigue specimens

Initial Disbond Lengths (mm)	No.	Total Measured Cycles (cycles)	Cycles Prior to Initial Growth (cycles)	Last Measured Crack Lengths (mm)	Avg. Crack Growth Rate (mm/cycle)	Failure Mode
60	1	15,052	3000	Left: 68.1 Right: 61.8	Left: 5.06×10^{-4} Right: 1.31×10^{-4}	Central Adherend
60	2	55,299	2000	Left: 95.3 Right: 64.6	Left: 7.19×10^{-4} Right: 9.52×10^{-5}	Central Adherend
60	3	41,996	5000	Left: 86.9 Right: 64.6	Left: 8.86×10^{-4} Right: 1.14×10^{-4}	Central Adherend
120	1	12,080	1000	Left: 133.5 Right: 121.1	Left: 4.37×10^{-4} Right: 9.26×10^{-5}	Central Adherend
120	2	60,500	10,000	Left: 165.0 Right: 122.5	Left: 9.11×10^{-4} Right: 6.00×10^{-5}	Bond Failure

technique (VCCT), which is based on linear elastic fracture mechanics. Therefore, all three materials were modelled as perfectly elastic materials – only the mechanical properties of the FM 73 were altered for these models. For the energy release rate models, the left side of the joint in Fig. 4 was fixed, while a pressure of 262.2 MPa (33.3 kN) was applied to the end of the aluminium central adherend. In the calculation, the VCCT method was implemented through the extended finite element method (XFEM), which introduces enriched nodes with additional degrees of freedom [40,41]. Another benefit of implementing XFEM is its ability to simulate propagation without a predefined crack path, should future work warrant crack path predictions. XFEM cracks in each of the tapers were modelled by embedding and allocating 2D planes of specific lengths within the adhesive centreline.

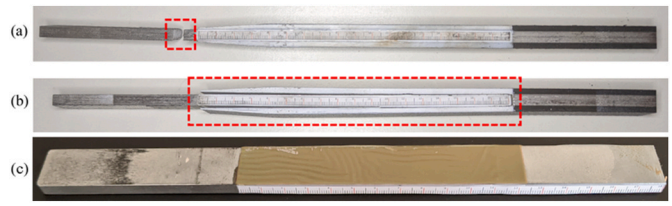

Fig. 6. Two failure modes: a) aluminium central adherend failure, b) bond failure, and c) fracture surface of bond failure specimen.

4. Results and discussion

As per the framework, the measured static residual strengths were used to calibrate the numerical models for residual strength predictions through the characteristic distance method. The predicted residual strength with knock-down factors and aluminium strength requirements determined the upper limit of the fatigue peak load for joint safe operation under fatigue loading. Crack growth rates measured from the fatigue tests and the energy release rates calculated from additional finite element models were used to establish a modified Paris law.

4.1. Static testing results

Initially, static tests were conducted on double laps with 60 and 120 mm disbond cracks originating from the taper end. The testing of these specimens resulted in aluminium central adherend failure, therefore specimens with 165-mm disbond cracks were static tested to obtain the force needed for bond failure. Fig. 5 illustrates the force-displacement curves for two specimens with a 165-mm disbond crack originating from the taper end. The averaged residual strength was 18.2 kN. As stated in Section 3.2, this experimentally measured residual strength was used to calibrate the element size in the numerical models through the characteristic distance method.

4.2. Fatigue testing results

Table 4 contains the measured crack propagation data and the recorded cycle numbers upon specimen failure. For the specimens specific to this study, the growing disbond crack was labelled as the “left” side while the stagnant disbond crack was labelled as the “right” side of the double lap joint. Two of the specimens, “60 mm No. 1” and “120 mm No. 1”, displayed fewer cycles at the peak load of 33.3 kN. As the first specimens of their respective configurations, the fatigue peak load was incrementally increased following a similar procedure to that presented by Wang et al. [4]. Starting from 27 kN, the load was incremented by 2 kN after 10,000 cycles of negligible disbond crack propagation (27, 29, 31, 33.3 kN). The incremental load increase was a conservative approach to minimise the risk of the specimen failing immediately, should 33.3 kN be too high. The focus of the study is the slow-growth damage behaviour which occurs after crack initiation. While the total measured cycles influence the fatigue life of the aluminium adherend, the life assessment of the aluminium is not within the scope of this research. As such, the cycle count prior to natural disbond growth is considered irrelevant. Fig. 6 illustrates the two failure modes from the fatigue testing. For all but one of the specimens, the aluminium central adherend failed before the taper disbond crack propagated along the entire 180-mm overlap length. The 12,000–60,000 cycles for the specimens in this study fall within the vicinity of non-dynamic aircraft components under typical severe fatigue loading conditions [42,43]. Bond failure was a mixture between cohesion and thin-layer cohesion failure. On the metallic surface of the central adherend, there was a thin layer of residual adhesive material. When comparing the failure modes of composite-metal double lap joints with metal-metal double lap joints presented by Tanulia et al. [28], it is evident that the composite outer

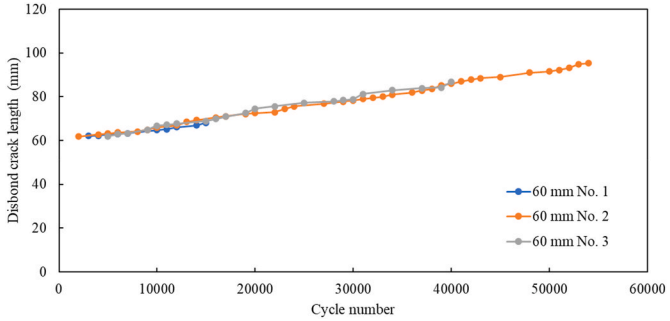

Fig. 7. Disbond crack length vs. cycle number for 60 mm initial taper disbond cracks.

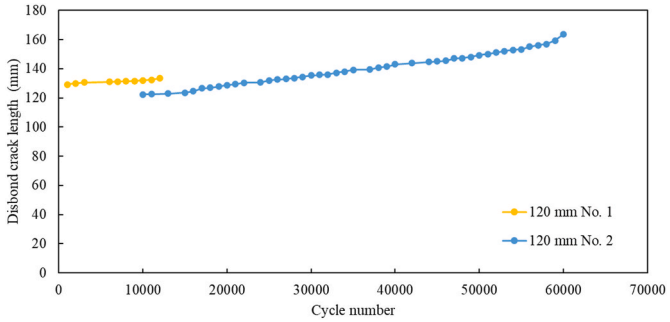

Fig. 8. Disbond crack length vs. cycle number for 120 mm initial taper disbond cracks.

adherends in this study did not fail by the gap region. This is most likely due to the longer fatigue life of the CFRP compared to the Al 7050-T7451. Specimen "120 mm No. 2" exhibited bond failure. In all tests, crack migration from disbond to delamination was not observed, which was also reported in a paper previously [26]. Since bonded composite joints often experience first-ply failure in static loading tests at room temperature [44], this highlights an important distinction in the failure behaviour of joints under static and fatigue loading conditions for a joint configuration considered in this study.

Since aluminium failure was the limiting factor in most of the specimens, joints with disbond cracks of 60 and 120 mm were needed to assess a sufficiently wide portion of the overlap length. Figs. 7 and 8 detail the progression of the crack growth with respect to the cycle number for specimens with a disbond of 60 and 120 mm originating from the taper end, respectively. Towards the end of the specimen "120 mm No. 2", an acceleration in crack growth can be found from cycles 58,000–60,000. This is indicative of a transition from a consistently growing crack to an accelerating crack.

4.3. Numerical modelling results

As described in Section 3.2, a characteristic distance method was used to calibrate the prediction against measured residual strength. An element size of 0.125 mm yielded a residual strength prediction of 18.5 kN compared to the averaged experimental residual strength of 18.2 kN for a joint with a 165-mm taper disbond crack. Additionally, the static tests for specimens with taper disbond cracks of 60 and 120 mm resulted in aluminium failure with a maximum load of approximately 65.0 kN. As such, the residual strengths at these disbond cracks were, at minimum, 65.0 kN. The element size of 0.125 mm yielded a predicted strength of 65.7 and 64.0 kN for 60 and 120 mm disbond crack lengths, respectively.

The calculated residual strength for composite-metal hybrid double lap joints with varying disbond lengths originating from the taper end is

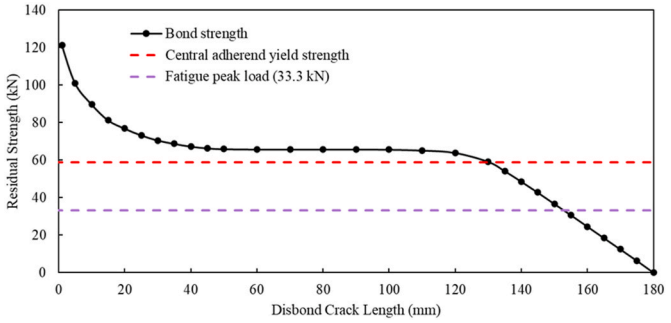

Fig. 9. Residual strength based on taper disbond crack length.

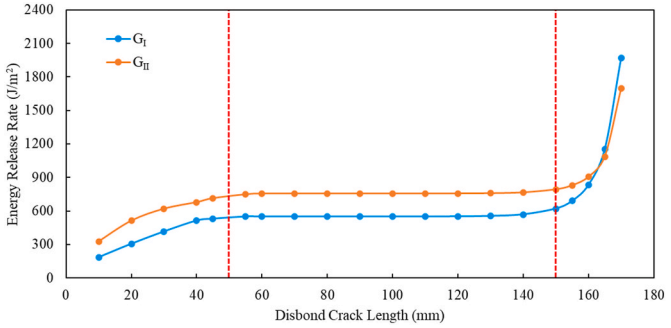

Fig. 10. G_I and G_{II} energy release rates for symmetrical taper disbond cracks.

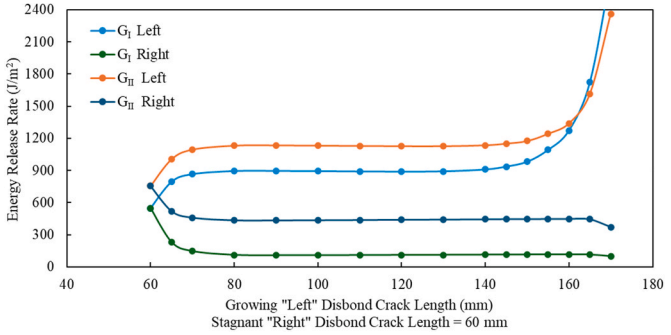

Fig. 11. G_I and G_{II} energy release rate for asymmetrical taper disbond cracks.

shown in Fig. 9. The load at which the aluminium yields is indicated by the red line, above which, the yielding of the aluminium central adherend would occur before bond failure. A peak load of 33.3 kN produces a critical crack length of approximately 153 mm, beyond which, the joint would subsequently fail.

Phase I crack growth displays characteristics of the crack initiation, Phase II of stable crack growth, and Phase III of unstable growth/fracture [45]. Fig. 10 illustrates the G_I (opening) and G_{II} (in-plane shear) energy release rates for double lap joints with symmetrical crack growth. For these symmetrical double lap joints, Phase I growth occurs between 0 and 50 mm, Phase II growth between 50 and 150 mm, and Phase III growth after 150 mm. It is worth noting that the crack lengths for the crack propagation phases are not identical between the residual strength prediction (Fig. 9) and the energy release rate prediction (Fig. 10). During Phase II growth, the mixed mode ratio (G_{II}/G_T) was approximately 0.58. G_{II} energy release rates maintain a higher magnitude compared to G_I for disbond crack lengths of 0–162 mm. Since the critical energy release rate G_{Ic} is smaller than G_{IIc} (Table 3), the threshold for the mode I failure is proportionally lower compared to the mode II failure.

Table 5
G_I and G_{II} energy release rates (ERR) for 60-mm disbond, disbond delamination, or delamination cracks

Damage Scenarios	Disbond crack G_I ERR (J/m^2)	Disbond crack G_{II} ERR (J/m^2)	Delam. crack G_I ERR (J/m^2)	Delam. crack G_{II} ERR (J/m^2)
60 mm Disbond only	548.8	754.6	–	–
60 mm Disbond with 0.25 mm Delamination	481.4	645.9	0	10.3
60 mm Delamination only	–	–	131.3	134.1

Fig. 11 depicts the G_I and G_{II} energy release rates for double lap joints with asymmetrical disbond crack growth, where one crack length is a stagnant 60 mm and the other extends from 60 to 170 mm. The energy release rates for both crack tips were included. The energy release rates of the stagnant disbond crack length trends towards 0 while those of the growing disbond crack length increases. As stated in Section 4.2, the "growing" and "stagnant" disbond cracks in this study were labelled as the "left" and "right" sides of the double lap joint, respectively. During Phase II growth, the mixed mode ratios were 0.56 and 0.80 for the growing 'left' side and the stagnant 'right' side, respectively. Asymmetrical crack growth causes the double-lap joint to bend towards the side with the shorter crack. This leads to the side with the longer crack (left in this study) to have an increased G_I (opening) component. As G_{IC} is lower than G_{IIC} (Table 3), G_I fracture is considerably more damaging to the double-lap joint. This explains why continued asymmetrical crack growth was observed in the experimental studies.

Finite element models of the bonded composite-metal hybrid double lap joints with co-existing disbond and delamination cracks were also created to help understand the non-migratory behaviour of the taper end disbond cracks. Table 5 lists the G_I and G_{II} energy release rates for the bonded joints with three different damage scenarios, namely disbond, delamination, and 60-mm disbond cracks migrated to first-ply delamination. The coexistence of disbond and delamination cracks significantly decreased the energy release rates at the delamination crack tip, while it had a relatively small effect on those at the disbond crack tip. The higher energy release rate at the disbond crack compared to the delamination crack indicates that a disbond crack will continue to grow, even in the presence of a crack migration from disbond to first-ply delamination. The dominance of disbond propagation, despite the presence of delamination cracks, provides insight into why crack migration from disbond to delamination was not observed in the fatigue studies.

5. Fatigue life predictions using a Modified Paris Law

The Paris law equation [46] is frequently used as the basis for predicting fatigue crack growth:

$$\frac{da}{dN} = C\Delta K^n \tag{1}$$

where, $\frac{da}{dN}$ is the experimentally measured growth of a crack length a for a cycle N. C and n are experimentally derived material constants and $\Delta K = (K_{max} - K_{min})$ is the stress intensity factor range. When assessing the failure of adhesives and fibre-reinforced composites, energy release rate G is typically used instead of the stress intensity factor [28]. As such, an adaptation of this equation is one which uses G instead of K:

$$\frac{da}{dN} = \delta\left(\frac{\Delta G_I}{G_{Ic}}\right)^{\alpha} + \gamma\left(\frac{\Delta G_{II}}{G_{IIc}}\right)^{\beta} \tag{2}$$

where, α, δ, β, and γ are experimentally derived constants. G_{Ic} and G_{IIc} are the critical energy release rates of the material and $\Delta G = (G_{max} - G_{min})$ is calculated based on the energy release rates at the crack tip from the finite element analyses.

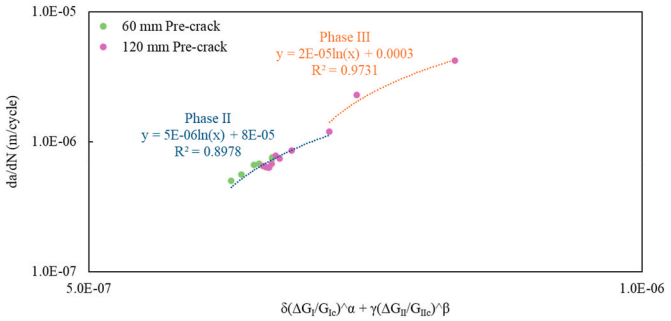

Fig. 12. Fatigue crack growth plots for a disbond crack (Blue line represents Phase II growth and orange line represents Phase III growth).

Table 6
α, δ, β, and γ parameters of the Paris law equation (Eq. (2))

α	δ	β	γ
4.15	1.3E-06	0.37	1.1E-06

A modified Paris law is established by correlating experimentally measured crack growth rates with the numerically calculated energy release rates for the bonded composite-metal hybrid double lap joint, as shown in Fig. 12. The blue data points represent the sampled intervals during Phase II propagation, while the orange are the final three intervals measured from the "120 mm No. 2" specimen, which exhibited characteristics of initial Phase III propagation. This is supported by Fig. 8 where cycle numbers 58,000–60,000 of specimen "120 mm No. 2" displayed an acceleration in the growth of the disbond crack. Through the least squares method, the α, δ, β, and γ variables crucial for Eq. (2), were determined and listed in Table 6.

Fatigue life predictions are attained using Eq. (2), along with the α, δ, β, and γ parameters (Table 6), numerically calculated energy release rates for joints with asymmetrical disbond cracks (Fig. 11), and the critical energy release rates of the FM 73 film adhesive (Table 3). Table 7 details the measured fatigue life from the experimental studies and the predicted fatigue life calculated using the modified Paris law equation. The predicted fatigue life is limited by the joint residual strength based on the peak load of 33.3 kN, which is correlated with a disbond crack length of 153 mm (Fig. 9). This means that the prediction for specimen "120 mm No. 2" only accounts for the growth of the disbond crack between lengths 120–153 mm. If a commonly considered retrospective NDI management approach is considered [47], that sets inspection intervals at 50 % of the remaining safe life (number of cycles the component is expected to withstand), providing an adequate safety margin when translating predicted fatigue life to realistic inspection regimes. The predicted fatigue life for all specimens in this study show adequate tolerance to this criterion.

6. Conclusions

This study investigates the slow-growth damage of bonded composite-metal hybrid double lap joints with disbond cracks originating from the taper end via experimental and numerical studies. Static tension tests yielded the residual strength of the double lap joints. The static residual strength and characteristic distance method was used to calibrate the numerical models for predicting residual strengths for disbond cracks along the overlap length (0–180 mm). Constant amplitude fatigue tests with a load within the range for realistic applications were conducted to assess the fatigue life and crack growth rates for the double lap joints. Further numerical models with XFEM and VCCT were developed to predict the energy release rates at the disbond cracks. A

Table 7
Measured and predicted fatigue life of the double lap joint

Initial Disbond Lengths (mm)	No.	Last Measured Crack Lengths (mm)	Total Measured Cycles (cycles)	Cycles Prior to Initial Growth (cycles)	Measured Fatigue Life[a] (cycles)	Predicted Fatigue Life[b] (cycles)	50 % of Predicted Fatigue Life (cycles)
60	1	Left: 68.1 Right: 61.8	15,052	3000	12,052	13,898	6949
60	2	Left: 95.3 Right: 64.6	55,299	2000	53,299	52,426	26,213
60	3	Left: 86.9 Right: 64.6	41,996	5000	36,996	40,668	20,334
120	1	Left: 133.5 Right: 121.1	12,080	1000	11,080	18,958	9479
120	2	Left: 165.0 Right: 122.5	60,500	10,000	50,500	45,228	22,614

[a] Measured Fatigue Life = Total Measured Cycles - Cycles Prior to Initial Growth.
[b] Limited by the joint residual strength reaching the peak load of 33.3 kN.

modified Paris law, used to predict fatigue life, is established using the experimental crack growth rates and the numerically predicted energy release rates.

The key findings from this research are detailed below.

- Under fatigue loading, the failure was only observed within the aluminium central adherend or within the adhesive. The composite outer adherends in the composite-metal hybrid double lap joints of this study did not experience failure.
- Under fatigue loading, the initial taper end disbond cracks within the adhesive layers did not migrate to delamination in the composite. This behaviour can be explained by using numerical models with disbond migrated to first-ply delamination cracks. With both disbond and delamination crack fronts, energy release rates at the disbond crack were considerably higher than those at the delamination crack.
- Slow-growth behaviours were observed until a disbond crack length of 150 mm out of an overlap length of 180 mm for this double lap joint, suggesting that the slow-growth management approach is applicable to a significant portion of the overlap length.
- The modified Paris law is established to predict fatigue life by correlating the experimental crack growth rates with the numerically calculated energy release rates. Predicted fatigue life using this modified Paris law agrees very well with that from the experiments.

The study in this paper focuses on disbond cracks originating from the taper end of the composite-metal double lap joint. Composite-metal double lap joints with disbond cracks originating from the gap region, as well as delamination cracks from the taper end and gap region should be further investigated as future work. Due to the prevalence of aluminium adherend failure, future specimens will require several pre-embedded crack lengths to assess a sufficiently wide range of the overlap length. Future work also includes assessing the slow-growth damage behaviour of composite-composite single-strap joints under compression loading by following the procedure outlined in this study.

CRediT authorship contribution statement

Laurence Wong: Writing – original draft, Validation, Methodology, Investigation, Formal analysis, Data curation, Conceptualization. **John Wang:** Writing – review & editing, Supervision, Resources, Methodology, Funding acquisition, Conceptualization. **Richard Chunhui Yang:** Writing – review & editing, Supervision, Software, Resources, Methodology, Funding acquisition. **Y.X. Zhang:** Writing – review & editing, Supervision, Resources, Project administration, Methodology, Funding acquisition, Conceptualization.

Declaration of competing interest

The authors declare that they have no known competing financial interests or personal relationships that could have appeared to influence the work reported in this paper.

Acknowledgements

The authors would like to acknowledge the technical support from Mr. Jinan Cao from the Forburn Pty Ltd and Mr. Robert Marshall from the Structural Testing Laboratory of Western Sydney University. Department of Defence of Australian Government provided fund support and Defence Science and Technology Group (DSTG) provided access to materials and facilities for specimen manufacturing.

Data availability

Data will be made available on request.

References

[1] Baker A, Chester R, Mazza J. Bonded repair technology for aging aircraft. Ageing mechanisms and control specialists' meeting on life management techniques for ageing air vehicles. 2003, ADP014082.
[2] Soykok I. End geometry and pin-hole effects on axially loaded adhesively bonded composite joints. Compos B Eng 2015;77:129–38. https://doi.org/10.1016/j.compositesb.2015.03.031.
[3] Alam P, Mamalis D, Robert C, Floreani C, Ó Brádaigh CM. The fatigue of carbon fibre reinforced plastics – a review. Compos B Eng 2019;166:555–79. https://doi.org/10.1016/j.compositesb.2019.02.016.
[4] Wang J, Rider AN, Heller M, Kaye R. Theoretical and experimental research into optimal edge taper of bonded repair patches subject to fatigue loadings. Int J Adhesion Adhes 2005;25:410–26. https://doi.org/10.1016/j.ijadhadh.2004.11.007.
[5] Omairey S, Jayasree N, Kazilas M. Defects and uncertainties of adhesively bonded composite joints. SN Appl Sci 2021;3:769. https://doi.org/10.1007/s42452-021-04753-8.
[6] Federal Aviation Administration. Composite aircraft structure. U.S. Department of Transportation; 2010. AC20-107B, Change 1.
[7] Federal Aviation Administration. Damage tolerance and fatigue evaluation of structure. U.S. Department of Transportation; 2017. FAR 23.573.
[8] SAE International. Composite materials handbook, vol. 17; 2012. CMH-17-1G.
[9] Baker A, Scott ML. Composite materials for aircraft structures. third edition; 2016.
[10] Chalkley P, Wang C, Baker A. Fatigue testing of generic bonded joints. Advances in the bonded composite repair of metallic aircraft structure. 2002. p. 103–26.
[11] Ashcroft IA, Casas-Rodriguez JP, Silberschmidt VV. A model to predict the anomalous fatigue crack growth behaviour seen in mixed mechanism fracture. J Adhes 2010;86:522–38. https://doi.org/10.1080/00218464.2010.484306.
[12] Bernasconi A, Beretta S, Moroni F, Pirondi A. Local stress analysis of the fatigue behaviour of adhesively bonded thick composite laminates. J Adhes 2010;86:480–500. https://doi.org/10.1080/00218464.2010.484300.
[13] Bisagni C, Furfari D, Pacchione M. Experimental investigation of reinforced bonded joints for composite laminates. J Compos Mater 2017;52:431–47. https://doi.org/10.1177/0021998317708021.
[14] Zhan X, Chen S, Li Y, Wang H, Yang Y. Effect of surface cold ablation on shear strength of CFRP adhesively bonded joint after UV laser treatment. Int J Adhesion Adhes 2019;94:13–23. https://doi.org/10.1016/j.ijadhadh.2019.05.006.
[15] Grundmann N, Brüning H, Tserpes K, Strohbach T, Mayer B. Influence of embedding fiber optical sensors in CFRP film adhesive joints on bond strength. Sensors 2020;20:1665. https://doi.org/10.3390/s20061665.
[16] Liu X, Zheng G, Luo Q, Li Q, Sun G. Fatigue behavior of carbon fibre reinforced plastic and aluminum single-lap adhesive joints after the transverse pre-impact. Int J Fatig 2021;144:105973. https://doi.org/10.1016/j.ijfatigue.2020.105973.

[17] Fernández MV, de Moura MFSF, da Silva LFM, Marques AT. Composite bonded joints under mode I fatigue loading. Int J Adhesion Adhes 2011;31:280–5. https://doi.org/10.1016/j.ijadhadh.2010.10.003.
[18] Campilho RDSG, M da Silva LF. Mode I fatigue and fracture behaviour of adhesively-bonded carbon fibre-reinforced polymer (CFRP) composite joints. Fatigue and fracture of adhesively-bonded composite joints. 2015. p. 93–120.
[19] Tserpes K, Floros I. Fatigue crack growth simulation in adhesively bonded composite joints. Fatig Fract Eng Mater Struct 2018;42:1430–40. https://doi.org/10.1111/ffe.12969.
[20] Floros I, Tserpes K. Fatigue crack growth characterization in adhesive CFRP joints. Compos Struct 2019;207:531–6. https://doi.org/10.1016/j.compstruct.2018.09.020.
[21] Bello I, Alowayed Y, Albinmousa J, Lubineau G, Merah N. Fatigue crack growth in laser-treated adhesively bonded composite joints: an experimental examination. Int J Adhesion Adhes 2021;105:102784. https://doi.org/10.1016/j.ijadhadh.2020.102784.
[22] Villamil AAB, Casas-Rodriguez JP, Holguin AP, Barrera MS. Mode I crack propagation experimental analysis of adhesive bonded joints comprising glass fibre composite material under impact and constant amplitude fatigue loading. Materials 2021;14:4380. https://doi.org/10.3390/ma14164380.
[23] Pan W, Sun L, Wei J, Zhang Y, Gao X, Wang J. Fatigue failure prediction method and constant amplitude equivalence strategy of adhesive interface under variable amplitude loading. Int J Adhesion Adhes 2024;129:103586. https://doi.org/10.1016/j.ijadhadh.2023.103586.
[24] Demiral M, Mamedov A. Fatigue performance of a step-lap joint under tensile load: a numerical study. Polymers 2023;15:1949. https://doi.org/10.3390/polym15081949.
[25] Kubit A, Macek W, Zielecki W, Szawara P, Myśliwiec P. Experimental study of the impact of notches and holes made in the front edge of adherends on the properties of static and fatigue strength of adhesive joints. Int J Adhesion Adhes 2024;129:103596. https://doi.org/10.1016/j.ijadhadh.2023.103596.
[26] Wu C, Gunnion AJ, Chen B, Yan W. Fatigue damage tolerance of two tapered composite patch configurations. Compos Struct 2015;134:654–62. https://doi.org/10.1016/j.compstruct.2015.08.114.
[27] Tanulia V, Wang J, Pearce GM, Baker A, David M, Prusty BG. A procedure to assess disbond growth and determine fatigue life of bonded joints and patch repairs for primary aircraft structures. Int J Fatig 2020;137:105664. https://doi.org/10.1016/j.ijfatigue.2020.105664.
[28] Tanulia V, Wang J, Pearce GM, Baker A, Chang P, Prusty BG. Experimental and computational assessment of disbond growth and fatigue life of bonded joints and patch repairs for primary airframe structures. Int J Fatig 2022;159:106776. https://doi.org/10.1016/j.ijfatigue.2022.106776.
[29] Baumann A, Hausmann J. Compression fatigue testing setups for composites – a review. Adv Eng Mater 2021;23:2000646. https://doi.org/10.1002/adem.202000646.
[30] Kabir MI, Wong L, Wang J, Yang C, Zhang YX. Slow growth damage assessment of bonded metal-composite joint using a numerical approach. International Journal of Applied Mechanics 2023;15:2250082. https://doi.org/10.1142/S175882512250082X.
[31] Wong L, Kabir MI, Wang J, Zhang YX, Yang C. Numerical slow growth damage assessment of an adhesively bonded composite joint under compression through four-point bending. Int J Comput Methods 2023;15:2241006. https://doi.org/10.1142/S0219876222410067.
[32] Hayes-Griss JM, Orifici AC, Khatibi AA. An improved progressive failure modelling and damage tolerant design methodology for composite scarf joints with bondline flaws. Compos Appl Sci Manuf 2020;131:105776. https://doi.org/10.1016/j.compositesa.2020.105776.
[33] Iarve EV, Hoos K, Braginsky M, Zhou E, Mollenhauer DH. Progressive failure simulation in laminated composites under fatigue loading by using discrete damage modeling. J Compos Mater 2016;51:2143–61. https://doi.org/10.1177/0021998316681831.
[34] Aydin MD. 3-D nonlinear stress analysis on adhesively bonded single lap composite joints with different ply stacking sequences. J Adhes 2008;84:15–36. https://doi.org/10.1080/00218460801888359.
[35] Sugiman S, Crocombe AD, Ashcroft IA. Experimental and numerical investigation of the static response of environmentally aged adhesively bonded joints. Int J Adhesion Adhes 2013;40:224–37. https://doi.org/10.1016/j.ijadhadh.2012.08.007.
[36] Rider A, Chalkley P. Durability of an off-optimum cured aluminium joint. Int J Adhesion Adhes 2004;24:95–106. https://doi.org/10.1016/S0143-7496(03)00102-7.
[37] Al-Rubaie KS, Del Grande MA, Travessa DN, Cardoso KR. Effect of pre-strain on the fatigue life of 7050-T7451 aluminium alloy. Materials Science and Engineering: A 2007;464:141–50. https://doi.org/10.1016/j.msea.2007.02.024.
[38] Whitney JM, Nuismer RJ. Stress fracture criteria for laminated composites containing stress concentrations. J Compos Mater 1974;8:253–65. https://doi.org/10.1177/002199837400800303.
[39] Wang J, Banbury A, Kelly D. Evaluation of approaches for determining design allowables for bolted joints in laminated composites. Journal of Composite Structures 1998;41:167–76. https://doi.org/10.1016/S0263-8223(98)00053-1.
[40] Abaqus. 10.7.1 Modeling discontinuities as an enriched feature using the extended finite element method. ABAQUS Analysis User's Guide 2016.
[41] Curiel-Sosa JL, Brighenti R, Serna Moreno MC, Barbieri E. Computational techniques for simulation of damage and failure in composite materials. Structural Integrity and Durability of Advanced Composites 2015:199–219.
[42] Baker AA, Gunnion AJ, Wang J, Chang P. Advances in the proof test for certification of bonded repairs – increasing the technology readiness level. Int J Adhesion Adhes 2016;64:128–41. https://doi.org/10.1016/j.ijadhadh.2015.10.008.
[43] Baker AA. Boron/epoxy patching efficiency studies [Chapter 13]. In: Baker AA, Rose LRF, Jones R, editors. Advances in the bonded composite repair of metallic aircraft structure. London, UK: Elsevier; 2002.
[44] Karthikeyan N, Naveen J. Progress in adhesive-bonded composite joints: a comprehensive review. J Reinforc Plast Compos 2021:1–47. https://doi.org/10.1177/07316844241248236.
[45] Tudose LM, Popa CO. Stress intensity factors analysis on cracks in the Hertzian stresses field of teeth gears. ROTRIB'07; 2007.
[46] Paris P, Erdogan F. A critical analysis of crack propagation laws. Journal of Basic Engineering 1963;85:528–33. https://doi.org/10.1115/1.3656900.
[47] Baker A, Wang J. Proposed through-life management approaches for adhesively bonded repair of primary structures. Int J Adhesion Adhes 2018;87:151–63. https://doi.org/10.1016/j.ijadhadh.2018.10.001.